Inorganic Chemistry

Article

pubs.acs.org/IC

Defusing Complexity in Intermetallics: How Covalently Shared Electron Pairs Stabilize the FCC Variant $Mo_2Cu_xGa_{6-x}$ ($x \approx 0.9$)

Brandon J. Kilduff, Vincent J. Yannello, and Daniel C. Fredrickson*

Department of Chemistry, University of Wisconsin—Madison, 1101 University Avenue, Madison, Wisconsin 53706, United States

Supporting Information

ABSTRACT: Simple sphere packings of metallic atoms are generally assumed to exhibit highly delocalized bonding, often visualized in terms of a lattice of metal cations immersed in an electron gas. In this Article, we present a compound that demonstrates how covalently shared electron pairs can, in fact, play a key role in the stability of such structures: $Mo_2Cu_xGa_{6-x}$ ($x \approx 0.9$). $Mo_2Cu_xGa_{6-x}$ adopts a variant of the common $TiAl_3$ structure type, which itself is a binary coloring of the fcc lattice. Electronic structure calculations trace the formation of this compound to a magic electron count of 14 electrons/T atom (T = transition metal) for the $TiAl_3$ type, for which the Fermi energy coincides with an electronic pseudogap. This count is one electron/T atom lower than the electron concentration for a hypothetical $MoGa_3$ phase, making this structure less competitive relative to more complex alternatives. The favorable 14 electron count can be reached, however, through the partial substitution of Ga with Cu. Using DFT-calibrated Hückel calculations and the reversed approximation Molecular Orbital (raMO) method, we show that the favorability of the 14 electron count has a simple structural origin in terms of the 18 − n rule of T−E intermetallics (E = main group element): the T atoms of the $TiAl_3$ type are arranged into square nets whose edges are bridged by E atoms. The presence of shared electron pairs along these T−T contacts allows for 18 electron configurations to be achieved on the T atoms despite possessing only 18 − 4 = 14 electrons/T atom. This bonding scheme provides a rationale for the observed stability range of $TiAl_3$ type TE_3 phases of ca. 13−14 electrons/T atom, and demonstrates how the concept of the covalent bond can extend even to the most metallic of structure types.

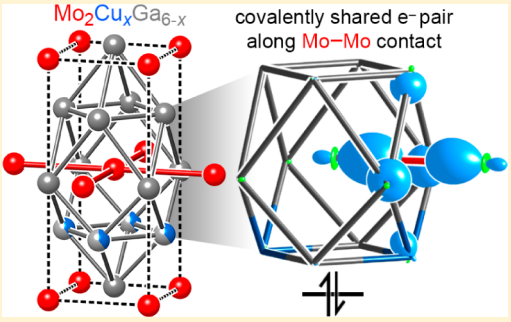

1. INTRODUCTION

Of the three fundamental types of bonding—covalent, ionic, and metallic—the metallic bond has been uniquely difficult to grasp from the chemical point of view. This difficulty is made vivid by the early attempts to draw resonance structures for simple elemental metals such as Li, wherein frustration quickly arises through the extremely low ratio of electrons to close interatomic contacts (1:7 for bcc alkali metals).[1,2] An intractable number of possible resonance structures is the result. The bonding in such systems has been more satisfyingly viewed in terms of free electrons that are weakly perturbed by the presence of a lattice of cations. While different from the way chemists usually approach bonding (though not entirely incompatible with it),[3,4] this idea has immense power: it forms the basis of the Mott−Jones model for Hume−Rothery phases[5] and motivates the use of plane waves as a basis-set for quantum mechanical calculations on periodic solids.[6,7]

From the successes of the nearly free electron model over a localized view of bonding in simple metals, it is tempting to consider the concept of the covalently shared electron pair as completely foreign to structures based on fcc, bcc, or hcp atomic packings. In this Article, we present a counterexample to this expectation, with the synthesis, crystal structure, and bonding analysis of the new phase $Mo_2Cu_xGa_{6-x}$ ($x \approx 0.9$), hereafter referred to as $Mo_2Cu_{0.9}Ga_{5.1}$. This phase exhibits a disordered variant of the $HfCuSi_2$ type,[8] which is itself a variant of the $TiAl_3$ type,[9] all of which are colorings of the fcc structure.

The simplicity of the $Mo_2Cu_{0.9}Ga_{5.1}$ structure is in stark contrast to the intriguing intermetallic phase Mo_8Ga_{41} that inspired our investigations into the Mo−Cu−Ga system. Mo_8Ga_{41} crystallizes in the V_8Ga_{41} structure type,[10,11] in which a primitive cubic lattice of Ga atoms serves as a host to guest clusters of transition-metal-capped $Ga@Ga_{12}$ cuboctahedra.[12] Small variations of the composition of this phase have been found to lead to variations on this host−guest theme. In Mo_6Ga_{31}[13] and $Mo_8Ga_{40.88}S_{0.86}$,[14] dimers and columns of such guest clusters were observed embedded in a similar host matrix, and more extensive structural chemistry was revealed in the structure of $V_{11}Cu_9Ga_{46}$ by Lux et al.[15] Based on these observations, we were interested in how the addition of Cu to the Mo−Ga system could influence these host−guest type arrangements. In the structure of $Mo_2Cu_{0.9}Ga_{5.1}$, the answer appears to be the suppression of structural complexity in favor of more simple atomic packing.

As we will see below, a bonding analysis of $Mo_2Cu_{0.9}Ga_{5.1}$ (and related phases) offers a simple explanation for how Cu substitution in the Mo−Ga system brings these results. DFT

Received: June 13, 2015
Published: July 27, 2015

DOI: 10.1021/acs.inorgchem.5b01333
Inorg. Chem. 2015, 54, 8103−8110

calculations reveal that, as in other compounds based on the $TiAl_3$ type,[16−21] this phase exhibits a pronounced electronic pseudogap at the valence electron count of 14 electrons/transition metal (T) atom, indicative of special stability. Using the reversed approximation Molecular Orbital (raMO) method,[22] we trace this pseudogap to the filling of 18 electron configurations on the T atoms, achieved with the help of shared electron pairs along four T−T contacts at each T center. In this way, the phase becomes an example of the recently proposed $18 - n$ rule for intermetallics.[23]

Without Cu, a hypothetical $TiAl_3$-type $MoGa_3$ phase would overshoot the preferred 14 electron/T count by one electron/T atom, making this structure less energetically competitive in a Ga-rich melt relative to complex structures such as Mo_8Ga_{41}. Substitution with Cu, however, offers the ability to lower the valence electron count back towards its optimal value. In this way, the existence of $Mo_2Cu_{0.9}Ga_{5.1}$ reveals how covalently shared electron pairs can stabilize even the most archetypal of metallic structures.

2. EXPERIMENTAL SECTION

Synthesis. Samples of $Mo_2Cu_xGa_{6-x}$ where x = 0.5, 1.0, 1.5, and 2.0 were prepared by combining loose powders of Mo (Strem Chemical, 99.95%) and Cu (Strem Chemicals, 99.9%) with ingots of Ga (Strem Chemical, 99.99%) into Al_2O_3 crucibles in an Ar filled glovebox. The crucibles were then lowered into fused silica tubes, which were transferred to a vacuum line (with precautions taken to avoid exposure to atmospheric O_2), where they were evacuated to ∼95 mTorr and sealed with a torch. The sealed tubes were then placed on-end in a muffle furnace and heated from room temperature to 800 °C over 4 h, held at 800 °C for 96 h, and cooled to room temperature over 80 h. A nearly phase pure sample of $Mo_2Cu_{0.9}Ga_{5.1}$ was prepared by arc melting a pellet of composition $Mo_2Cu_{0.75}Ga_{5.25}$ (a slight excess of Ga was used to compensate for the potential loss of Ga during pellet pressing and arc melting), sealing it in an evacuated fused silica tube, and annealing it in a muffle furnace using the same heating profile as described above.

Single Crystal X-ray Diffraction Analysis. Single crystal X-ray diffraction analysis was performed on a crystal picked from the sample with loading composition $Mo_2Cu_xGa_{6-x}$ ($x \approx 1.0$), where the phase appeared in the largest yield as indicated from powder X-ray diffraction data. Data were collected on an Oxford Diffraction Xcalibur E diffractometer using graphite monochromatized Mo Kα radiation (λ = 0.710 73 Å) at ambient temperature. Run list optimization and data processing were performed using the CrysAlis Pro ver. 171.36.28 software supplied by the manufacturer. The structure was solved with the charge flipping algorithm[24,25] using the program SUPERFLIP.[26] The solution was refined using JANA2006[27] by full matrix least-squares on F^2, which yielded (when combined with compositional information from EDS) a structure of composition $Mo_2Cu_{0.9}Ga_{5.1}$. Further information concerning the crystal data is given in Table 1, while details of the refinement are provided in the Supporting Information.

Powder X-ray Diffraction Analysis. Samples were ground into fine powders using an agate mortar and pestle, and mounted onto a zero-background plate. Diffraction intensities were collected with a Bruker D8 Advance Powder Diffractometer using Cu Kα radiation (λ = 1.5418 Å) at room temperature. The measurements employed a LYNXEYE detector and an exposure time of 0.6 s per 0.01° for the 2θ range 15−90°. The diffraction patterns were analyzed using Match! version 2.2.2 and JANA2006. Loading compositions with x = 0.5, 1.0, and 1.5 displayed peaks agreeing with the calculated $Mo_2Cu_{0.9}Ga_{5.1}$ pattern. The unit cells of $Mo_2Cu_xGa_{6-x}$ for each loading composition were determined from the powder patterns using a least-squares refinement implemented in UNITCELL.[28] Shifts in the diffraction peaks between x = 0.5 and 1.5 indicated a contraction of a = 0.007 Å and expansion of c = 0.013 Å for larger values of x, indicating a small phase width for Cu substitution. For x = 0.5, large quantities of Mo_3Ga and $Mo_2Cu_3Ga_5$, as well as a small amount of Mo_8Ga_{41}, could be identified as impurities. At x = 1.0, $Mo_2Cu_xGa_{6-x}$, Mo_3Ga, and $Mo_2Cu_3Ga_5$ were identified in agreement with SEM-EDS analysis. For loading compositions above x = 1.0 an unidentified phase began to form with a peak at 2θ = 40.38°. Powder diffraction patterns are provided in the Supporting Information (Figures S1 and S2).

Table 1. Crystallographic Information for $Mo_2Cu_{0.9}Ga_{5.1}$

chemical formula	$Mo_2Cu_{0.9}Ga_{5.1}$[a]
EDS composition	$Mo_2Cu_{0.84(9)}Ga_{5.25(22)}$
space group	$P4/nmm$
a (Å)	3.69830(10)
c (Å)	8.6170(2)
cell volume	117.858(5)
Z	1
Pearson symbol	$tP8$
cryst dimensions (mm^3)	0.03 × 0.05 × 0.07
cryst color	metallic gray
cryst shape	irregular
data collection temp	RT
radiation source, λ (Å)	Mo, Kα (0.7107)
abs coeff (mm^{-1})	37.606
abs corr	analytical[29]
min/max transm	0.203, 0.408
θ_{min}, θ_{max}	4.73, 32.42
no. reflns	2340
$R_{int}[I > 3\sigma(I)]$, R_{int}(all)	2.53, 2.55
unique ref [$I > 3\sigma(I)$, all]	141,155
no. params	12
$R[I > 3\sigma(I)]$, $R_w[I > 3\sigma(I)]$	1.48, 3.93
R(all), R_w(all)	1.75, 4.08
$S[I > 3\sigma(I)]$, S(all)	1.18, 1.20
$\Delta\rho_{max}$, $\Delta\rho_{min}$ ($e^-/Å^3$)	0.72, −0.86

[a]The chemical formula formula was determined as follows: The Mo:(Cu/Ga) ratio was determined from single crystal X-ray diffraction results, while the Cu/Ga ratio (which is difficult to determine from diffraction data due to the similar form factors of Cu and Ga for Mo, Kα radiation) was estimated from SEM-EDS results of the sample from which the single crystal was taken.

Energy Dispersive X-ray Spectroscopy. Samples were prepared for elemental analysis using energy dispersive X-ray spectroscopy (EDS) by suspending fragments of the reaction products in nonconductive epoxy in a hollow Al bullet. Once the epoxy had hardened, the surface was polished with diamond lapping film (down to a 0.5 μm grit) until cross sections of the crystals were visible under a light microscope. The samples were then sonicated for ∼60 s in isopropanol to remove any surface contamination from polishing, allowed to dry in air, and then coated by evaporation with a 200 Å thick layer of carbon to avoid charging in an electron beam. The $Mo_2Cu_xGa_{6-x}$ samples were examined with a Hitachi S-3100N scanning electron microscope equipped with an EDS probe (15 kV). There were 20−30 points measured on each sample. For samples with x = 0.5, 1.0, and 1.5, three phases were identified corresponding to Mo_3Ga, $Mo_2Cu_3Ga_8$, and $Mo_2Cu_xGa_{6-x}$. For x = 2.0 only compositions corresponding to Mo_3Ga and $Mo_2Cu_3Ga_8$ were found. The average composition of $Mo_2Cu_xGa_{6-x}$, excluding carbon, was determined from the Mo L-shell, Ga Kα-shell, and Cu Kα-shell emission lines. The compositions of the $Mo_2Cu_xGa_{6-x}$ phase were determined to be $Mo_{1.92(3)}Cu_{0.76(9)}Ga_{5.32(23)}$, $Mo_{1.91(3)}Cu_{0.84(9)}Ga_{5.25(22)}$, and $Mo_{1.93(3)}Cu_{0.94(9)}Ga_{5.13(23)}$ for loading compositions with x = 0.5, 1.0, and 1.5, respectively. While the three compositions appear to show a correlation between Cu content and x, the observed variation in composition across the series is within the error bars of the measurements. The homogeneity range of this phase is thus narrower than the precision of the EDS results.

DOI: 10.1021/acs.inorgchem.5b01333
Inorg. Chem. 2015, 54, 8103−8110

DFT-Calibrated Hückel Calculations. To provide a basis for the creation of Hückel models for $Mo_2Cu_{0.9}Ga_{5.1}$ (approximated as Mo_2CuGa_5 to obtain an ordered structure), $NbGa_3$, and a hypothetical $TiAl_3$-type $MoGa_3$ phase, electronic structure calculations were carried out on their structures using the Vienna ab initio Simulation Package (VASP).[30,31] First, the crystal structures were geometrically optimized, and then the DFT band energies and electronic density of states (DOS) distributions of the obtained structures were computed. All VASP calculations were performed in the high-precision mode, using the GGA ultrasoft pseudopotentials[32] provided with the package. 12 ×12 × 5 and 13 × 13 × 5 Γ-centered k-point grids were used for the $TiAl_3$-type and Mo_2CuGa_5 structures, respectively (see the Supporting Information for further details).

Simple Hückel parameters were then refined from the output of the VASP calculations using the program eHtuner,[33] with the Hückel calculations themselves being carried out with a modified version of YAeHMOP.[34] The optimized Hückel parameters can be found in the Supporting Information, along with the RMS deviations between the band energies of the Hückel models and those calculated with VASP (all <0.2 eV).

Following the refinement of the Hückel parameters, Hückel DOS curves were calculated, and preparations were made for a reversed approximation Molecular Orbital (raMO) analysis[22] by performing Hückel calculations on 4 × 4 × 2 supercells of the structures, so that several of the special k points of the primitive cells were mapped to the Γ points. The Hamiltonian matrix for the Γ point of each supercell was printed and imported into MATLAB, where the raMO analysis was carried out using a series of in-house functions.

3. RESULTS AND DISCUSSION

3.1. The Crystal Structure of $Mo_2Cu_{0.9}Ga_{5.1}$. During our syntheses in the Mo−Cu−Ga system, we obtained crystals whose diffraction patterns were consistent with a tetragonal cell of dimensions a = 3.70 Å and c = 8.62 Å. These cell dimensions are suggestive of the $TiAl_3$ structure type adopted by a number of 1:3 transition metal (T) gallides.[35−38] A closer look at reciprocal lattice reconstructions of the single crystal diffraction data indicated that the strongest reflections indeed follow the $h + k + l = 2n$ condition expected for the $I4/mmm$ space group of the $TiAl_3$ type. However, weaker reflections were also present violating this systematic absence law, indicating that a superstructure pattern breaking the I-centering of the original structure type is present. Inspection of the remaining systematic absences suggested $P4/nmm$ as the highest space group symmetry consistent with the diffraction pattern. This choice was confirmed in the subsequent steps of the structure solution and refinement, which yielded a structure of composition $Mo_2Cu_{0.9}Ga_{5.1}$.

As expected from these cell parameters, the crystal structure of this phase is closely related to the $TiAl_3$ structure type (Figure 1a). The $TiAl_3$ type itself can be simply derived by considering an fcc lattice of Al atoms, doubling the unit cell along c, and finally replacing the corner and central Al atoms of the supercell with Ti atoms. In $Mo_2Cu_{0.9}Ga_{5.1}$, Mo and Ga/Cu atoms take positions analogous to those of the Ti and Al in the $TiAl_3$ type, respectively (Figure 1b,c). However, the placement of Ga and Cu among the Al-type sites is not uniform. The Cu atoms are largely restricted to the $z = {}^3/_4$ layer of the $TiAl_3$ structure, with the remainder of the Al-type sites occupied by Ga. Full occupation of the $z = {}^3/_4$ sites with Cu would correspond to the $HfCuSi_2$ structure type, but the X-ray diffraction data indicate that this layer consists of mixed Ga/Cu sites, with the EDS results suggesting that the ratio is approximately 45 Cu:55 Ga. The placement of Cu onto this site agrees with DFT-calculations; only models with Cu substituted onto the $z = {}^3/_4$ layer resulted in the observed crystal geometry when structurally optimized (see section S2 of the Supporting Information).

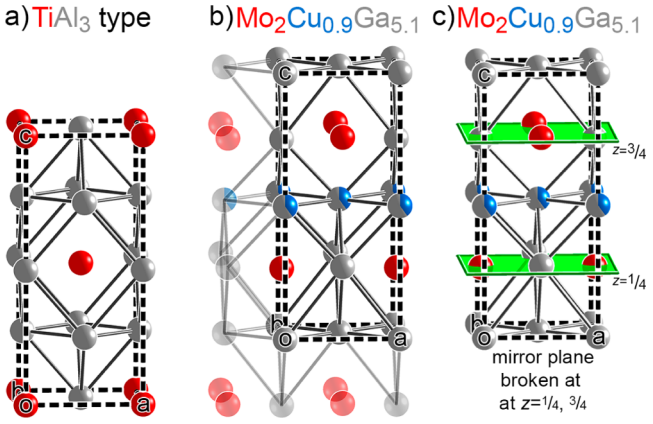

Figure 1. The crystal structure of $Mo_2Cu_{0.9}Ga_{5.1}$, a ternary variant of the $TiAl_3$ structure type. (a) The $TiAl_3$ structure type. (b) An expanded view of the $Mo_2Cu_{0.9}Ga_{5.1}$ structure illustrating its relationship to the $TiAl_3$ type. The Ga atoms, originally at $z = {}^3/_4$, are mixed with approximately 45% Cu. This substitution breaks the body centering of the $TiAl_3$ type cell leading to the primitive unit cell of $Mo_2Cu_{0.9}Ga_{5.1}$ shown. (c) One unit cell of the $Mo_2Cu_{0.9}Ga_{5.1}$ structure.

This substitution of a single layer in the unit cell with Cu breaks both the I-centering of the original $TiAl_3$ type, and the mirror planes passing through the transition metal atoms perpendicular to the c-axis. This change in symmetry leads to a shift in the unit-cell origin by $(0, {}^1/_2, {}^1/_4)$, as shown in Figure 1b. The new origin places the Cu-substituted layer prominently in the center of the unit cell along c. The lower symmetry of this arrangement means that the Mo and Ga atoms in the planes above and below the Cu-substituted layer are no longer held at fixed positions as they were in the $TiAl_3$ type cell. They are now free to move along the c-axis in response to the fact that they have Cu/Ga mixed sites on one side of them along c, but only Ga atoms on the other. In these motions, the Mo atoms retreat away from the Cu-substituted layer while the Ga atoms advance toward the Cu substitution (Figure 1c).

3.2. Electronic Pseudogaps in $Mo_2Cu_{0.9}Ga_{5.1}$ and $TiAl_3$-Type Phases. The structural analysis above illustrates how the addition of Cu to a Ga-rich Mo−Ga melt leads to the formation of a simple $TiAl_3$ type variant rather than the significantly more complex Mo_8Ga_{41} phase. An important clue to the origins of $Mo_2Cu_{0.9}Ga_{5.1}$ is the observation that while $MoGa_3$ does not exist,[39] a $TiAl_3$-type phase does form when we move from Mo to Nb: $NbGa_3$.[38] This observation can be rationalized by a comparison of the electronic density of states (DOS) distributions calculated for $NbGa_3$ and a hypothetical $TiAl_3$-type $MoGa_3$ phase (Figure 2a,b) using a DFT-calibrated Hückel model (see the Experimental Section for details). The Fermi energy (E_F) of the $NbGa_3$ structure sits comfortably in a pseudogap in the structure's electronic DOS distribution, as has been noted previously.[21] This matching of the E_F at the structure's electron count of 14/T atom with a pseudogap is an indication of a favorable electron count, just as large HOMO−LUMO gaps are correlated with stability in molecules. This expectation is confirmed by an examination of the binary T−E intermetallics listed as crystallizing in the $TiAl_3$ type by the Inorganic Crystal Structure Database (ICSD).[40−42] The vast

DOI: 10.1021/acs.inorgchem.5b01333
Inorg. Chem. 2015, 54, 8103−8110

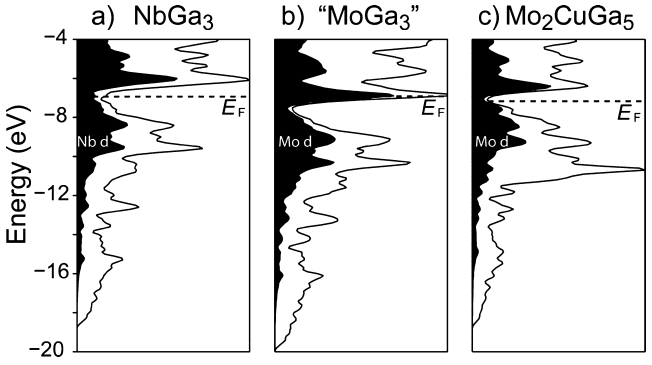

Figure 2. DFT-calibrated Hückel DOS distributions of (a) $TiAl_3$-type $NbGa_3$, (b) a hypothetical $MoGa_3$ phase in the $TiAl_3$ type, and (c) an ordered model of $Mo_2Cu_{0.9}Ga_{5.1}$. The DOS contributions from the Nb and Mo d-states are shaded in black. (See Figure S3 in the Supporting Information for GGA-DFT versions of these curves.)

majority exhibit valence electron counts in the range of 13−14 electrons/T atom.

On moving from $NbGa_3$ to the hypothetical $MoGa_3$ structure, the DOS distribution is largely unchanged, with an analogous pseudogap still occurring at 14 electrons/T atom. However, the replacement of Nb with Mo has increased the phase's electron count from 14 to 15 electrons/T atom. As a consequence, the E_F now occurs above the pseudogap (Figure 2b). A $TiAl_3$ type $MoGa_3$ phase would thus be in excess of the structure's preferred electron count by 1 electron per T atom.

The partial substitution of Ga with Cu offers an opportunity to remedy this electron excess, as Cu atoms have two fewer electrons than Ga ones. Indeed, moving from $MoGa_3$ to Mo_2CuGa_5 (very close to the experimental composition of $Mo_2Cu_{0.9}Ga_{5.1}$) restores the valence electron count to 14 electrons/Mo atom. Such is confirmed by a calculation on an ordered model of this phase (with Cu and Ga atoms placed in a checkerboard pattern in the $z = 0.5$ layer). For this Mo_2CuGa_5 structure, the E_F lies once again in the DOS pseudogap (Figure 2c).

3.3. Localized Bonding Scheme from a reversed approximation Molecular Orbital Analysis. From this analysis, we see that restoring the valence electron count to 14 electrons/T atom appears to be important to the preference of this Mo−Cu−Ga phase for a $TiAl_3$-type structure. The favorability of this electron count for the $TiAl_3$ type has previously been rationalized with an innovative extension of Wade's rules to the Al sublattice, after which interactions with the T atoms are introduced (see section 3.4 for additional discussion).[20] In this section, we will see how focusing on the T sublattice instead can fold these compounds into a more general electron counting rule for intermetallics, the $18 - n$ rule.

The basis of our analysis is the recently developed reversed approximation Molecular Orbital (raMO) approach,[22] which offers a way to directly connect local structural features to preferred electron counts. In this method, the occupied crystal orbitals of a compound are used as a basis set for constructing a local MO diagram for a portion of a structure. For T−E intermetallics, we have found that a powerful MO diagram for this purpose is the 9 bonding and nonbonding levels of an 18 electron transition metal complex, whose MOs are templated by the nine s, p, and d valence atomic orbitals of the T center. Such an MO diagram can be extracted from the wave functions of an intermetallic by using the valence atomic orbitals of one of its T atoms as target states, and using the raMO procedure to obtain the best orthogonal approximations to these states that can be constructed from linear combinations of the occupied crystal orbitals.

In Figure 3, we show the results of applying this method to $NbGa_3$, using the 4d-, 5s-, and 5p-orbitals of a Nb atom as target eigenstates. In examining the resulting raMO orbitals, we see that, for each Nb valence atomic orbital, a corresponding raMO function appears that is centered by that orbital.

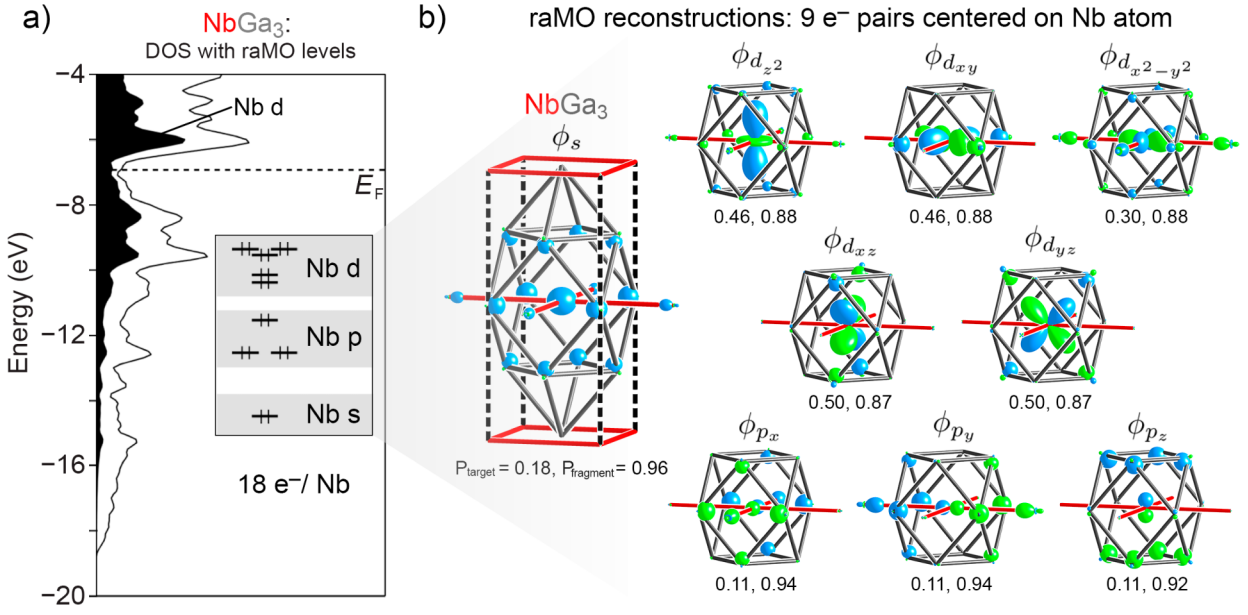

Figure 3. raMO reconstructions of a single Nb atom's s-, p-, and d-orbitals in $NbGa_3$. (a) Energies of the raMO levels drawn alongside the DOS distribution of the phase. (b) The raMO functions. σ contributions can be seen from the atom's Ga and Nb nearest neighbors. The quantities P_{target} and $P_{fragment}$ supply information about the degree of each raMO's localization, by giving the probability of finding a raMO's electrons in, respectively, the target orbital and the structural fragment displayed in the image.

DOI: 10.1021/acs.inorgchem.5b01333
Inorg. Chem. 2015, 54, 8103−8110

However, in each case the target orbital is accompanied by in-phase contributions on the surrounding atoms, which indicate the presence of bonding interactions.

Strong σ type interactions between the central Nb atom and its Ga neighbors are common to all of the raMOs. However, the balance in the functions between the Nb and Ga atoms (as is measured by the probability of finding a raMO's electrons on the target orbital, P_{target}) varies depending on whether the orbital is based on a Nb s-, p-, or d-orbital. The low P_{target} values for the Nb s and p reconstructions suggest their raMOs are heavily polarized toward the Ga neighbors. The values of P_{target} are notably higher for the Nb d-orbitals (≈0.5), indicating that the probability of finding an electron on the Nb atom is larger for these functions. These results are in accord with the relative energies of the Nb s, p, and d: the Nb 4d-orbitals being lower in energy contributes more to the Nb−Ga bonding states than the Nb 5s- or 5p-orbitals.

Some of the raMO functions also exhibit features that are less familiar to molecular chemistry. On the s-, p_x-, p_y-, and $d_{x^2-y^2}$-centered raMO reconstructions, significant in-phase σ-contributions from the neighboring Nb atoms are present (Figure 4a).[43] The appearance of bonding overlap at these Nb−Nb contacts is rather unexpected as the Nb−Nb distance of 3.79 Å (in the GGA-DFT optimized structure) is far too long to be considered as a traditional through-space Nb−Nb bond. The appearance of such interactions, despite the long interatomic distances, is made more understandable by turning our attention to the orbital contributions from the Ga atoms around the Nb−Nb contacts. Each Nb−Nb contact is bridged by a square of Ga atoms (corresponding to one of the square faces of the Ga_{12} cuboctahedron of the Nb coordination environment), which provide σ bonding lobes to support the overlap between the Nb atoms.

The appearance of four bonding Nb−Nb functions for four Nb−Nb contacts around the central Nb atom suggests the possibility of obtaining more localized functions. In fact, the combination of s-, p_x-, p_y-, and $d_{x^2-y^2}$-orbitals is exactly the set of orbitals needed for the creation of sp^2d hybrid orbitals on a transition metal center for pointing to the vertices of a square planar complex.[2] In Figure 4b, we take the proper linear combinations of these raMOs to create such hybrids. Four localized functions result, each corresponding to a multicenter interaction isolobal to a standard Nb−Nb σ bond, and (as they are constructed from linear combinations of occupied functions) are populated by two electrons. The appearance of such electron pairs at main-group-bridged T−T contacts places the $TiAl_3$ type into a growing family of intermetallics that use this mechanism to achieve closed shell electron configurations (examples include $Fe_8Al_{17.4}Si_{7.6}$,[44] $Co_3Al_4Si_2$,[45] $Ca_{10}Pt_7Si_3$,[46] Ir_3Ge_7 type,[22] and the Nowotny chimney ladders[23]).

As in these other phases, the T−T interactions in the $NbGa_3$ play a large role in determining its ideal electron count. Our raMO analysis indicates that there is an electron pair associated with each of the Nb valence orbitals, which suggests that the stability of the phase should be understandable from the point of view of filled 18 electron configurations on the Nb atoms.[47] However, the observed electron count is only 14 electrons/Nb atom, which is 4 electrons/Nb atom short of the number needed for independent Nb atoms. To solve this issue, each Nb atom shares electron pairs with four other Nb atoms. This is a specific instance of an $n = 4$ case of the more general $18 - n$ rule emerging for T−E intermetallics.

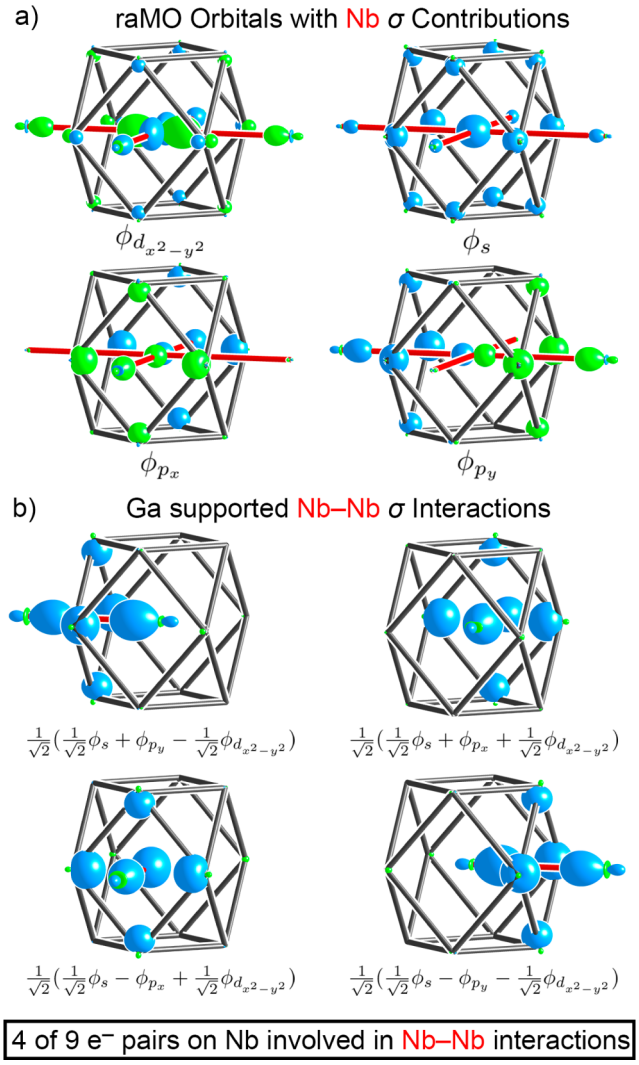

Figure 4. Covalently shared electron pairs along Nb−Nb contacts in $NbGa_3$. (a) raMO orbital reconstructions of raMOs exhibiting Nb−Nb bonding. (b) Localized linear combinations of the raMOs in part a chosen to create the sp^2d hybrid functions on the Nb center.

How would moving from $NbGa_3$ to $MoGa_3$, with its extra valence electron, affect this picture? To see this, it is helpful to focus in on one specific T−T σ bond, and examine how it is changed during this substitution. To do this we use a T−T σ bonding and antibonding pair of functions (Figure 5a) as target eigenstates for a new raMO analysis, and examine how the character and occupation of the resulting σ and σ^* functions change on going from $NbGa_3$ to the hypothetical $MoGa_3$ and finally to Mo_2CuGa_5. In Figure 5b−d, we compare the resulting raMO functions for the three phases.

Starting as before with $NbGa_3$ (Figure 5b), the σ bonding orbital is reproduced very well, and brings in supporting character from the bridging Ga atoms. The σ^* contribution, however, shows only a minuscule amount of occupation (P_{target} = 0.05), and the minor features present on the Nb atoms are hybridized away from the Nb−Nb contact in question. By expanding the fragment of the structure displayed to include two more Nb atoms in the chain, we see that, in attempting to reconstruct an antibonding function at the Nb−Nb contact, we in fact obtain an out-of-phase combination of bonding

DOI: 10.1021/acs.inorgchem.5b01333
Inorg. Chem. 2015, 54, 8103−8110

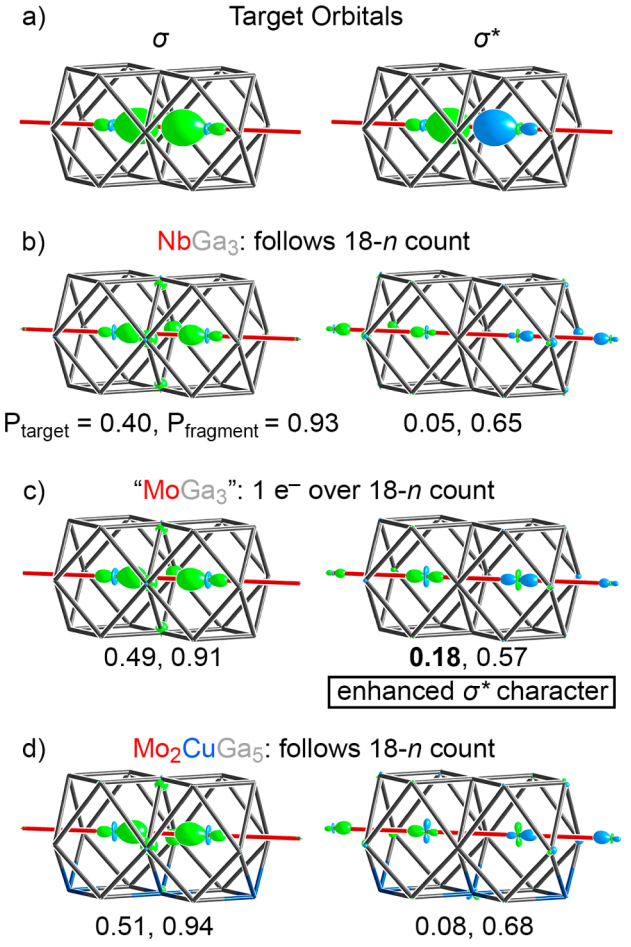

Figure 5. Reconstructions of σ and σ^* orbitals for a pair of T atoms in a series of structures based on the $TiAl_3$ type. raMO reconstructions of (a) the target eigenfunctions are shown for (b) $NbGa_3$, (c) a hypothetical $MoGa_3$ phase, and (d) Mo_2CuGa_5.

functions for the neighboring Nb−Nb contacts along the same chain.

As we move to the hypothetical $MoGa_3$ structure, the bonding picture changes (Figure 5c). The Mo−Mo σ raMO appears quite similar to that of $NbGa_3$; however, the σ^* combination is now reproduced much better (P_{target} = 0.18), and exhibits less hybridization away from the T−T contact. Additionally, the stabilizing contribution from the neighboring Mo atoms has decreased relative to Nb, suggesting that the σ antibonding interaction has become more localized between the Mo atoms. In effect, the extra valence electron/T atom injected into the system upon replacing Nb with Mo has resulted in an increased population of T−T σ^* states, and thus an overall disruption of bonding between the T atoms.

If adding electrons to the structure reduces the T−T bonding, removing these excess electrons should restore this bonding character. This is exactly what is observed in the raMO reconstructions of Mo_2CuGa_5 (Figure 5d). The T−T σ^* antibonding orbital is now once again poorly reproduced, and the stabilizing contributions from the neighboring T atoms have regained the magnitude seen in the $NbGa_3$ raMOs. Our raMO analysis of Mo_2CuGa_5 thus confirms our earlier picture of filled 18 electron configurations on the T atoms of the $TiAl_3$-type arising from shared electron pairs in T−T bonds.

In this section, we have seen a simple picture develop for bonding in T−E $TiAl_3$-type phases, as summarized in Figure 6.

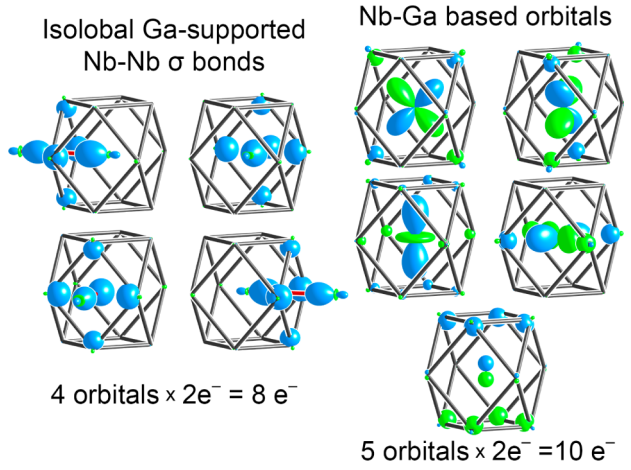

Figure 6. A summary of the electron counting scheme obtained for 14 electron $TiAl_3$-type phases, as exemplified by $NbGa_3$.

On each T atom, 5 electron pairs (in 4 d-orbitals and 1 p-orbital) are involved in bonding between the T and its E coordination environment. The 4 additional electron pairs (in functions built from the remaining valence atomic orbitals: s, p_x, p_y, and $d_{x^2-y^2}$) are shared in E-supported T−T bonds, one through each of the square faces of the E cuboctahedron in the *xy* plane. The result is the filling of 18 electron configurations on the T atoms at an electron count of 14/T atom.

This prediction of 14 electrons/T atom as a magic electron count for T−E $TiAl_3$-type phases coincides well with the upper limit of the observed range of ca. 13−14 electrons/T. How should this scheme be modified for the lower end of the electron count range? Our preliminary calculations suggest that moving to lower electron counts depopulates functions with the nodal character of T−T π^* functions. The removal of electrons relative to the 14 electron count could then be partially accommodated through the creation of net T−T π bonding interactions to supplement the T−T σ interactions already in place.

3.4. Comparison to Previous Bonding Schemes Proposed for the $TiAl_3$ Structure Type. How does this bonding model derived from raMO analysis compare with the results of other theoretical studies of $TiAl_3$-type structures? A common feature of most earlier analyses of the $TiAl_3$ type is the prominence of covalent interactions between the T and E atoms.[18,19,21,48] The raMO functions of Figures 3−6 confirm this conclusion, as each reconstruction of a T atomic orbital appears with substantial in-phase contributions from neighboring E atoms. This observation extends to the shared electron pairs along the T−T contacts, where the bridging E atoms play a key role in stabilizing the electron pairs.

Another point of comparison is how 14 electrons/T arises as the favorable electron count for the structure. Condron et al. provided a compelling explanation by conceptually building up the electronic structure through orbital considerations.[20] They began by demonstrating, through an extension of the Wade−Mingos rules, that the optimal electron count for the E-sublattice should be 10 electrons/formula unit. Next, they analyzed how the T valence orbitals would interact with the E-sublattice, finding that two d-orbitals per T atom (d_{z^2} and $d_{x^2-y^2}$) are available for occupation. These T d-orbitals provide

DOI: 10.1021/acs.inorgchem.5b01333
Inorg. Chem. 2015, 54, 8103−8110

room for the remaining four electrons/formula unit, so that the preferred electron count becomes 14 electrons/T atom.

In our T-centric, raMO-based approach the involvement of the T atom orbitals is different: they serve as templates for the nodal properties of the wave functions, rather than interacting with preformed E-based states. Given that we arrive at the same electron count, one might wonder whether these approaches, in the end, reduce to the same overall chemical picture. An important difference can be seen in the role the T $d_{x^2-y^2}$ function plays in the two models. In the E-centered picture, the T $d_{x^2-y^2}$-orbitals each host two electrons, precluding the possibility of bonding interactions between them. In the raMO-derived scheme, however, the T $d_{x^2-y^2}$-orbital appears as one of four T orbitals participating in the formation of the four T−T bonds around each T center. As such, the T $d_{x^2-y^2}$ functions would only be considered as having one rather than two electrons/T atom. In other words, the T−E and E-supported T−T interactions in these systems are sufficiently strong that a somewhat different electronic structure results than is derived assuming strong E−E interactions. As the raMO-based picture is derived from the occupied wave functions of $NbGa_3$ and Mo_2CuGa_5, it appears that its scheme is more representative of the bonding in these gallides.

4. CONCLUSIONS

In this Article, we have described a new phase, $Mo_2Cu_{0.9}Ga_{5.1}$, which serves as a clear counterexample to the electron gas bonding picture generally assumed for simple metallic lattices. This compound crystallizes in a colored fcc variant structure, in which the Mo atoms and Cu/Ga atoms are distributed to the Ti and Al positions in a $TiAl_3$-type lattice. The Cu and Ga atoms are then further resolved among the Al-type positions such that the Cu atoms partially substitute for Ga in half of the square nets of the structure. $Mo_2Cu_{0.9}Ga_{5.1}$ can thus be interpreted as a Cu-substituted derivative of the $TiAl_3$-type $MoGa_3$ phase, a hypothetical Mo analogue of the $TiAl_3$-type phase in the Nb−Ga system.

Through investigations into the bonding in $NbGa_3$ and $Mo_2Cu_{0.9}Ga_{5.1}$ we developed a simple picture for how Cu substitution stabilizes a $TiAl_3$-type phase not found in combinations of Mo and Ga on their own. DFT calculations revealed that these $TiAl_3$-based phases exhibit a pseudogap at the Fermi energy at 14 electrons per T atom. raMO analysis of these results using DFT-calibrated Hückel models traces this pseudogap to the filling of 18 electron configurations on the T atoms, which are achieved despite the electron count of 14 electrons/T atom, via multicenter interactions isolobal to four T−T σ bonds. While $MoGa_3$ in the $TiAl_3$-type deviates from this electron count with 15 electrons/Mo, the partial substitution of Ga with Cu lowers the valence electron concentration (VEC) back towards 14, reuniting the E_F with the pseudogap. The $TiAl_3$-type can thus be placed on the growing list of structures whose preferred electron counts can be understood in terms of the $18 - n$ rule, which includes 18 electron half Heusler compounds,[49,50] $Fe_8Al_{17.4}Si_{7.6}$,[44] $Co_3Al_4Si_2$,[45] the Ir_3Ge_7 type,[22] and the Nowotny chimney ladders.[23]

A second lesson offered by $Mo_2Cu_{0.9}Ga_{5.1}$ concerns the competition between simple and complex crystal structures in intermetallics. The Ga-rich part of the Mo−Ga phase diagram contains phases with relatively large unit cells, hinting at host−guest relationships. No simple binary structure seems to be available as a more stable alternative. However, the addition of a third element, Cu, serves to enhance the stability of one of these nominally binary structure types by offering extra flexibility to alleviate an unfavorable VEC. Examples of this effect in $TiAl_3$-type aluminides are prevalent: Mo_2CuAl_5,[51] W_2CuAl_5,[52] $ZrAl_2Si$,[53] and $MoCo_{0.28}Al_{2.72}$[54] are all described as adopting this structure type,[55] whereas the TAl_3 unsubstituted binaries either crystallize in more complex structures[9,56] or do not form.[57]

A parallel story involving sterics was encountered for the phases $Ca_2Cu_2Cd_9$ and Ca_5Cu_2Cd in our earlier exploration of the Ca−Cu−Cd system.[58] These structures are based off of binary structure types not found in any of the binary subsystems of the Ca−Cu−Cd ternary systems, a trend we connected to atomic packing issues. The addition of a third element expanded the palette of available atomic sizes, allowing the packing issues to be resolved. We are looking forward to exploring how other plausible but unobserved binary structures may be stabilized through the addition of some amount of a third element suggested by the theoretical evaluation of the factors limiting their stability. Promising systems for these investigations are binary systems exhibiting only complex structures, where significant bonding issues with simple alternative structures would be easiest to detect.

■ ASSOCIATED CONTENT

Supporting Information

Tables of crystallographic data for $Mo_2Cu_{0.9}Ga_{5.1}$, including atomic coordinates and interatomic distances; discussion of the assignment of Cu positions in the crystal structure of $Mo_2Cu_{0.9}Ga_{5.1}$; powder X-ray diffraction data; computational details; GGA-DFT optimized coordinates and total energies for $NbGa_3$, $MoGa_3$, and several ordered models of Mo_2CuGa_5; table of DFT-calibrated Hückel parameters used in this work; comparison of electronic DOS curves calculated with DFT and best-fit Hückel models; crystallographic information in CIF format. The Supporting Information is available free of charge on the ACS Publications website at DOI: 10.1021/acs.inorgchem.5b01333.

■ AUTHOR INFORMATION

Corresponding Author

*E-mail: danny@chem.wisc.edu.

Notes

The authors declare no competing financial interest.

■ ACKNOWLEDGMENTS

We thank Dr. John Fournelle for assistance with SEM-EDS measurements. We also gratefully acknowledge financial support from the National Science Foundation (NSF) through Grant DMR-1207409. B.J.K. thanks the NSF for a graduate student fellowship (Grant DGE-1256259). This research involved calculations using computer resources supported by NSF Grant CHE-0840494.

■ REFERENCES

(1) Pauling, L. *Proc. R. Soc. London, Ser. A* **1949**, *196*, 343−362.
(2) Pauling, L. *The Nature of the Chemical Bond*, 3rd ed.; Cornell University Press: Ithaca, NY, 1995.
(3) Anderson, W. P.; Burdett, J. K.; Czech, P. T. *J. Am. Chem. Soc.* **1994**, *116*, 8808−8809.
(4) Berger, R. F.; Walters, P. L.; Lee, S.; Hoffmann, R. *Chem. Rev.* **2011**, *111*, 4522−4545.

DOI: 10.1021/acs.inorgchem.5b01333
Inorg. Chem. 2015, 54, 8103−8110

(5) Mott, N. F.; Jones, H. *The Theory and Properties of Metals and Alloys*; Oxford University Press: Oxford, U.K., 1936.
(6) Ashcroft, N. W.; Mermin, N. D. *Solid State Physics*, 1st ed.; Holt, Rinehart and Winston: New York, 1976.
(7) Pettifor, D. G. *Bonding and Structure of Molecules and Solids*, 1st ed.; Oxford University Press: New York, 1995.
(8) Andruchiv, L. S.; Lysenko, L. O.; Yarmolyuk, Y. P.; Gladyshevskii, E. I. *Dopov. Akad. Nauk Ukr. RSR* **1975**, *A*, 645−648.
(9) Brauer, G. *Z. Anorg. Allg. Chem.* **1939**, *242*, 1−22.
(10) Yvon, K. *Acta Crystallogr., Sect. B: Struct. Crystallogr. Cryst. Chem.* **1975**, *31*, 117−120.
(11) Girgis, K.; Petter, W.; Pupp, G. *Acta Crystallogr., Sect. B: Struct. Crystallogr. Cryst. Chem.* **1975**, *31*, 113−116.
(12) Häussermann, U.; Viklund, P.; Svensson, C.; Eriksson, S.; Berastegui, P.; Lidin, S. *Angew. Chem., Int. Ed.* **1999**, *38*, 488−492.
(13) Yvon, K. *Acta Crystallogr., Sect. B: Struct. Crystallogr. Cryst. Chem.* **1974**, *30*, 853−861.
(14) Wołcyrz, M.; Andruszkiewicz, R.; Łukaszewicz, K. *Acta Crystallogr., Sect. C: Cryst. Struct. Commun.* **1989**, *45*, 991−993.
(15) Lux, R.; Kuntze, V.; Hillebrecht, H. *Solid State Sci.* **2012**, *14*, 1445−1453.
(16) Xu, J.-h.; Freeman, A. J. *Phys. Rev. B: Condens. Matter Mater. Phys.* **1989**, *40*, 11927−11930.
(17) Xu, J. H.; Freeman, A. J. *Phys. Rev. B: Condens. Matter Mater. Phys.* **1990**, *41*, 12553−12561.
(18) Hong, T.; Watson-Yang, T. J.; Freeman, A. J.; Oguchi, T.; Xu, J.-h. *Phys. Rev. B: Condens. Matter Mater. Phys.* **1990**, *41*, 12462−12467.
(19) Xu, J.-h.; Freeman, A. J. *J. Mater. Res.* **1991**, *6*, 1188−1199.
(20) Condron, C. L.; Miller, G. J.; Strand, J. D.; Bud'ko, S. L.; Canfield, P. C. *Inorg. Chem.* **2003**, *42*, 8371−8376.
(21) Lue, C. S.; Su, T. H.; Xie, B. X.; Cheng, C. *Phys. Rev. B: Condens. Matter Mater. Phys.* **2006**, *74*, 094101.
(22) Yannello, V. J.; Kilduff, B. J.; Fredrickson, D. C. *Inorg. Chem.* **2014**, *53*, 2730−2741.
(23) Yannello, V. J.; Fredrickson, D. C. *Inorg. Chem.* **2014**, *53*, 10627−10631.
(24) Oszlányi, G.; Sütő, A. *Acta Crystallogr., Sect. A: Found. Crystallogr.* **2004**, *60*, 134−141.
(25) Oszlányi, G.; Sütő, A. *Acta Crystallogr., Sect. A: Found. Crystallogr.* **2005**, *61*, 147−152.
(26) Palatinus, L.; Chapuis, G. *J. Appl. Crystallogr.* **2007**, *40*, 786−790.
(27) Petříček, V.; Dušek, M.; Palatinus, L. *Z. Kristallogr. - Cryst. Mater.* **2014**, *229*, 345−352.
(28) Holland, T. J. B.; Redfern, S. A. T. *Mineral. Mag.* **1997**, *61*, 65−77.
(29) Clark, R. C.; Reid, J. S. *Acta Crystallogr., Sect. A: Found. Crystallogr.* **1995**, *51*, 887−897.
(30) Kresse, G.; Furthmüller, J. *Phys. Rev. B: Condens. Matter Mater. Phys.* **1996**, *54*, 11169−11186.
(31) Kresse, G.; Furthmüller, J. *Comput. Mater. Sci.* **1996**, *6*, 15−50.
(32) Vanderbilt, D. *Phys. Rev. B: Condens. Matter Mater. Phys.* **1990**, *41*, 7892−7895.
(33) Stacey, T. E.; Fredrickson, D. C. *Dalton Trans* **2012**, *41*, 7801−7813.
(34) Landrum, G. A.; Glassey, W. V. *YAeHMOP: Yet Another extended Huckel Molecular Orbital Package*. YAeHMOP is freely available at http://sourceforge.net/projects/yaehmop/. Last accessed: June 11, 2015.
(35) Wallbaum, H. J. *Z. Metallkd.* **1942**, *34*, 118−119.
(36) Poetzschke, M.; Schubert, K. *Z. Metallkd.* **1962**, *53*, 474−488.
(37) Poetzschke, M.; Schubert, K. *Z. Metallkd.* **1962**, *53*, 548−560.
(38) Meissner, H. G.; Schubert, K. *Z. Metallkd.* **1965**, *56*, 475−484.
(39) Brewer, L.; Lamoreaux, R. H. *Mo-Ga Phase Diagram, ASM Phase Diagrams Database*; Villars, P., Editor-in-Chief; Okamoto, H., Cenzual, K., Section Editors; ASM International: Materials Park, OH, 2006. Last accessed: July 8, 2015.
(40) Bergerhoff, G.; Hundt, R.; Sievers, R.; Brown, I. D. *J. Chem. Inf. Model.* **1983**, *23*, 66−69.
(41) Bergerhoff, G.; Brown, I. D. In *Crystallographic Databases*; Allen, F. H., Bergerhoff, G., Sievers, R., Eds.; International Union of Crystallography: Chester, U.K., 1987; pp 77−95.
(42) Belsky, A.; Hellenbrandt, M.; Karen, V. L.; Luksch, P. *Acta Crystallogr., Sect. B: Struct. Sci.* **2002**, *58*, 364−369.
(43) Minor σ contributions from neighboring Nb atoms are also visible for the Nb d_{z^2} raMO. However, these only play a small role in the Nb−Nb interactions. This function has the same symmetry properties as the Nb s raMO, and their interaction would create one s-based function better optimized for Nb−Nb interactions, and a d_{z^2}-based function without Nb-Nb interactions
(44) Fredrickson, R. T.; Fredrickson, D. C. *Inorg. Chem.* **2012**, *51*, 10341−10349.
(45) Fredrickson, R. T.; Fredrickson, D. C. *Inorg. Chem.* **2013**, *52*, 3178−3189.
(46) Fredrickson, D. C.; Doverbratt, I.; Ponou, S.; Lidin, S. *Crystals* **2013**, *3*, 504−516.
(47) On the basis of the square planar hybridization we have evoked for the Nb center, one might wonder if a 16 electron count (as observed for molecular d^8 complexes) might be more appropriate. In those molecular square planar complexes, the out-of-plane T p-orbital remains unfilled as no bonding interactions occur to offset its high energy. In the case of $NbGa_3$, this p-orbital is heavily involved in bonding with the Ga atoms in the planes above and below, as is evident from its raMO function in Figure 3.
(48) Kavich, I. V.; Shcherba, I. D. *Metallofizika (Kiev)* **1981**, *3*, 38−42.
(49) Jung, D.; Koo, H. J.; Whangbo, M. H. *J. Mol. Struct.: THEOCHEM* **2000**, *527*, 113−119.
(50) Kandpal, H. C.; Felser, C.; Seshadri, R. *J. Phys. D: Appl. Phys.* **2006**, *39*, 776−785.
(51) Prevarskii, A. P.; Kuz'ma, Y. B.; Onyshkevich, M. M. *Metally* **1977**, *4*, 201−203.
(52) Prevarskii, A. P.; Kuz'ma, Y. B. *Metally* **1983**, *5*, 225−226.
(53) Schob, O.; Nowotny, H. N.; Benesovsky, F. *Monatsh. Chem.* **1961**, *92*, 1218−1226.
(54) Burnasheva, V. V.; Starodub, P. K.; Stroganov, G. B. *Metally* **1977**, *5*, 235−236.
(55) The structures of these compounds appear to have been assigned from powder X-ray diffraction data, where the superstructures similar to the one we have found for $Mo_2Cu_{0.9}Ga_{5.1}$ would be difficult to detect.
(56) Schuster, J. C.; Ipser, H. *Metall. Trans. A* **1991**, *22*, 1729−1736.
(57) Okamoto, H. *Al-W Phase Diagram, ASM Phase Diagrams Database*; Villars, P., Editor-in-Chief; Okamoto, H., Cenzual, K., Section Editors; ASM International: Materials Park, OH, 2006. Last accessed: July 8, 2015.
(58) Harris, N. A.; Hadler, A. B.; Fredrickson, D. C. *Z. Anorg. Allg. Chem.* **2011**, *637*, 1961−1974.

DOI: 10.1021/acs.inorgchem.5b01333
Inorg. Chem. 2015, 54, 8103−8110